

Optical tweezing chiral particles with 3D structured light

Kayn A. Forbes* and Dale Green

School of Chemistry, University of East Anglia, Norwich NR4 7TJ, United Kingdom

[*k.forbes@uea.ac.uk](mailto:k.forbes@uea.ac.uk)

ABSTRACT

In this work we highlight enantioselective optical gradient forces acting on Rayleigh-scattered chiral particles present in 3D structured (non-paraxial) optical vortex tweezing systems. One discriminatory force originates from the circular polarization of the light and is similar to previous chiral optical gradient trapping forces. Much more remarkable is the other which is independent of the input beam's polarization state - even occurring for unpolarized light - and is not present in 2D structured light nor propagating plane waves. This latter chiral sorting mechanism allows for the enantioselective trapping of chiral particles into distinct rings in the transverse plane through conservative radial forces.

Keywords: optical trapping, structured light, chirality, optical forces, optical manipulation, optical vortex, nano-optics, nanophotonics

1. INTRODUCTION

Light conveys energy and momentum, and this is the basis for optical manipulation of matter¹. Absorption and non-forward scattering of photons leads to a transfer of momentum and a radiation pressure force pushing particles in the direction of propagation. In classical theory this non-conservative force is often termed the scattering force. An alternative optical manipulation technique involves the forward Rayleigh scattering of photons, where the scattered photon is identical to the input one and as such no energy or momentum is transferred to the particle. In this case the particle experiences a conservative optical force which attracts it to regions of high optical intensity: this is known as the gradient force. Both the scattering force and gradient force are utilized in optical manipulation techniques, but it is the latter which proves most useful in general optical trapping schemes utilizing optical tweezers².

The dominant optical source in optical tweezers has long been an unstructured paraxial beam, a fundamental Gaussian mode for example. However, with the revolution in structured light sparked by the now renowned work carried out on optical vortices (also referred to as twisted light) in Leiden in 1992³, optical tweezers using twisted light has seen much activity⁴⁻⁶. The predominant reason for this is that they can transfer their orbital angular momentum (OAM) and induce mechanical motion of trapped particles. This transfer of OAM to cause rotational motion is completely distinct from the gradient trapping force itself; optical angular momentum is conserved in the gradient force. We refer⁷ to unstructured light as being homogenous in all spatial dimensions, the ubiquitous plane wave being a perfect example; 2D structured light is inhomogeneous (e.g. amplitude, phase, polarization) in the transverse (x,y) plane but homogenous along the direction of propagation z , its electromagnetic fields are purely transverse; 3D structured light is inhomogeneous in all directions and possesses significant longitudinal electromagnetic field components alongside the transverse components.

A distinct subdiscipline of optical trapping and tweezing of particles is the use of chiral light to trap chiral particles differentially depending on their material handedness. The basis of the principle is that a right-handed enantiomer will experience a different optical force than the left-handed form for a given input optical handedness, which in an initially racemic mixture would over time form a concentration gradient between the enantiomeric pair. The potential of sorting enantiomers using an all-optical method would have a profound impact on the drug and pharmaceutical industries, and as such there has been a substantial number of studies looking at enantioselective trapping schemes. These have predominantly involved using an unstructured laser source⁸⁻¹¹ and/or plasmonic enhancement systems¹²⁻²⁴, though there

have been a handful of studies employing structured light^{20,25–29}. Optical vortices are inherently chiral, their OAM per photon is $\ell\hbar$ where $\ell \in \mathbb{Z}$ is known as the topological charge. The sign of ℓ designates what direction the helical wavefront twists: for $\ell > 0$ it is left-handed, while $\ell < 0$ is right-handed. This chirality of the wavefront in optical vortices is analogous to the well-known optical chirality of circularly polarized light (CPL), where the quantity often referred to as the helicity $\sigma = +1$ corresponds to left-handed CPL and $\sigma = -1$ right-handed CPL, and the spin angular momentum (SAM) of CPL is given by $\sigma\hbar$. The chirality of optical vortices has witnessed a profusion of research activity, with the field recently surveyed³⁰. The question addressed in this paper is whether the OAM, both its sign (handedness) and magnitude, can influence the optical gradient trapping force when applied to Rayleigh-sized chiral particles under tight focusing.

2. CONSERVATIVE CHIRALITY-SORTING FORCES

Quantum electrodynamics³¹ (QED) is utilized to describe the light-matter interactions that correspond to the optical gradient forces acting on Rayleigh-sized particles in this paper. Truncated to the dipole approximation, the Power-Zineau-Woolley multipolar interaction Hamiltonian describes the coupling between light and matter³²:

$$H_{\text{int}}(\xi) = -\varepsilon_0^{-1} \mu_i(\xi) d_i^\perp(\mathbf{R}_\xi) - m_i(\xi) b_i(\mathbf{R}_\xi), \quad (1)$$

where $\mu_i(\xi)$ and $m_i(\xi)$ are the electric and magnetic dipole operators, respectively; $d_i^\perp(\mathbf{R}_\xi)$ and $b_i(\mathbf{R}_\xi)$ are the transverse (with respect to the Poynting vector) electric displacement field and magnetic field mode operators, respectively, acting on a particle ξ at the location \mathbf{R}_ξ ; Einstein summation of repeated tensor indices is assumed throughout, i.e. $a_i b_i = \mathbf{a} \cdot \mathbf{b}$. The first term in (1) is the electric dipole coupling (E1) and the second magnetic dipole coupling (M1). For input circularly-polarized Laguerre-Gaussian (LG) modes the electromagnetic free field expansion operators truncated to first-order in the paraxial parameter kw_0 may be given by^{33,34}

$$\mathbf{d}^\perp(\mathbf{r}) = i \sum_{k,\sigma,\ell,p} \left(\frac{\hbar ck \varepsilon_0}{2A_{\ell,p}^2 V} \right)^{1/2} \frac{1}{\sqrt{2}} \left[\left\{ (\hat{\mathbf{x}} + i\sigma\hat{\mathbf{y}}) + \frac{i}{k} \hat{\mathbf{z}} \left(\frac{\partial}{\partial r} - \ell \sigma \frac{1}{r} \right) e^{i\sigma\phi} \right\} f_{|\ell|,p}(r) a_{|\ell|,p}^{(\sigma)}(k\hat{\mathbf{z}}) e^{i(kz+\ell\phi)} - \text{H.c.} \right], \quad (2)$$

and

$$\mathbf{b}(\mathbf{r}) = i \sum_{k,\sigma,\ell,p} \left(\frac{\hbar k}{2c\varepsilon_0 A_{\ell,p}^2 V} \right)^{1/2} \frac{1}{\sqrt{2}} \left[\left\{ (\hat{\mathbf{y}} - i\sigma\hat{\mathbf{x}}) + \frac{1}{k} \hat{\mathbf{z}} \left(\sigma \frac{\partial}{\partial r} - \frac{\ell}{r} \right) e^{i\sigma\phi} \right\} f_{|\ell|,p}(r) a_{|\ell|,p}^{(\sigma)}(k\hat{\mathbf{z}}) e^{i(kz+\ell\phi)} - \text{H.c.} \right]. \quad (3)$$

where $k = 2\pi / \lambda$ is the wavenumber, V is a quantization volume, $A_{\ell,p}^2$ is a normalization constant for LG modes, $\sigma = \pm 1$, the positive sign designates left-handed CPL; the negative sign right-handed CPL, $a_{|\ell|,p}^{(\sigma)}(k\hat{z})$ is the annihilation operator, $\exp i(kz + \ell\phi)$ is the phase, $\ell \in \mathbb{Z}$ is the topological charge, H.c. stands for Hermitian conjugate, and $f_{|\ell|,p}(r)$ is the radial distribution function around the focal plane

$$f_{|\ell|,p}(r) = \frac{C_p^{|\ell|}}{w_0} \left(\frac{\sqrt{2}r}{w_0} \right)^{|\ell|} e^{-\frac{r^2}{w_0^2}} L_p^{|\ell|} \left[\frac{2r^2}{w_0^2} \right], \quad (4)$$

where w_0 is the beam waist, the normalization constant is given by $C_p^{|\ell|} = \sqrt{2p! / [\pi(p+|\ell|)!]}$ and $L_p^{|\ell|}$ is the generalised Laguerre polynomial of order p .

In (2) and (3), the terms that depend on \hat{x} and \hat{y} are the transverse components of the fields while those that depend on \hat{z} are the longitudinal components. 2D structured light possesses only the transverse components, whilst 3D structured light also has the longitudinal component. Furthermore, whilst the polarization state of 2D structured light is adequately described by 2D polarization theory, e.g. the four Stokes parameters, due to the fact all three spatial components of the field vectors (2) and (3) generally play a role in 3D structured light, the theory of polarization has been extended to the 3D case described by nine polarization parameters^{35,36}. To generate significant longitudinal field components, a 2D structured (paraxial) laser source is tightly focused using a high numerical aperture (NA) lens, producing 3D structured light at the focal plane. In this work we describe light by its source 2D polarization state and make clear whether it is paraxial (2D structured) or non-paraxial via tight focusing (3D structured).

The potential energy responsible for the optical gradient trapping force originates in forward Rayleigh scattering. In photonic terms, an input laser photon is annihilated at the particle and then an identical photon (same mode) is created at the same particle. This two photon interaction requires second-order perturbation theory to yield the leading order contribution to the potential energy¹:

$$U = \text{Re} \sum_R \frac{\langle I | H_{\text{int}} | R \rangle \langle R | H_{\text{int}} | I \rangle}{E_R - E_I}, \quad (5)$$

where the initial state of the system is given by $|I\rangle = |E_0(\xi); n(k, \sigma, \ell, p)\rangle$: the particle is in the ground state and the radiation field consists of n photons in the mode (k, σ, ℓ, p) ; the final state of the system is identical to the initial; the virtual intermediate state is given by $|R\rangle = |E_\alpha(\xi); (n-1)(k, \sigma, \ell, p)\rangle$.

Working strictly in the dipole regime the potential energy of a particle is then a sum of three distinct contributions:

$$U \simeq U_{\text{EIEI}} + U_{\text{EIMI}} + U_{\text{MIMI}}. \quad (6)$$

Chiral effects dependent on material handedness originate in the E1M1 term and so from now on we neglect the pure E1E1 and M1M1 effects as they are independent of material chirality³⁷.

3. 2D CIRCULARLY POLARIZED 3D LG MODE

With the aid of the Feynman graphs in Figure 1 and using (1) with the fields (2) and (3) in (5) produces the following potential energy for a 2D circularly polarized 3D LG beam:

$$U_{\text{E1M1}}^{\text{Circ}} = -\frac{I}{2\varepsilon_0 c^2} \text{Re} \left[\left\{ \bar{e}_i^\sigma f - \frac{i}{k} \left(f' - \frac{\ell \sigma}{r} f \right) e^{-i\sigma\phi} \hat{z}_i \right\} \left\{ b_j^\sigma f + \frac{1}{k} \left(\sigma f' - \frac{\ell}{r} f \right) e^{i\sigma\phi} \hat{z}_j \right\} G_{ij} + c.c. (i \leftrightarrow j) \right], \quad (7)$$

where we have dropped most dependencies for notational clarity, $c.c.(i \leftrightarrow j)$ stands for taking the complex conjugate and swapping the indices of the expression in brackets, $I = n\hbar c^2 k / A_{\ell,p}^2 V$ is the beam intensity, $f' = \partial_r f|_{\ell,p}(r)$, and the imaginary quantity referred to as the mixed electric-magnetic polarizability tensor (which has different signs for each chiral particle of an enantiomeric pair) is given explicitly as

$$G_{ij}(\omega, -\omega) = \sum_\alpha \left(\frac{\mu_i^{0\alpha} m_j^{\alpha 0}}{E_{\alpha 0} - \hbar\omega} + \frac{m_j^{0\alpha} \mu_i^{\alpha 0}}{E_{\alpha 0} + \hbar\omega} \right), \quad (8)$$

where the transition dipole moments are defined as $\mu_i^{0\alpha} (m_i^{\alpha 0}) = \langle E_0 | \mu_i (m_i) | E_\alpha \rangle$ and $E_{\alpha 0} = E_\alpha - E_0$.

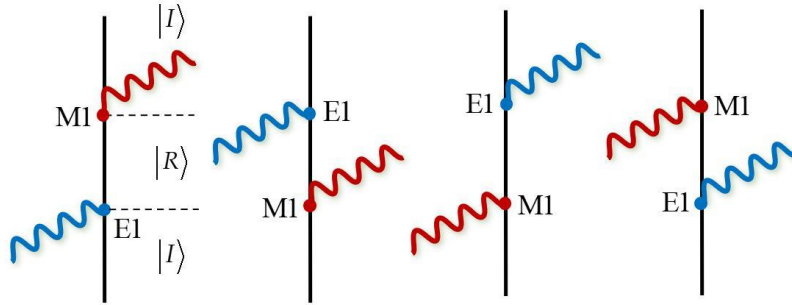


Figure 1: Topologically distinct Feynman diagrams for E1M1 forward Rayleigh scattering.

To account for the randomly oriented nature of chiral particles in the liquid or gas phase the potential energy must be rotationally averaged. Using well known methods³² in which each particle is decoupled from the space-fixed frame into the laboratory frame we produce

$$\langle U_{\text{EIMI}}^{\text{Circ}} \rangle = -\frac{I}{3\epsilon_0 c^2} \left[\sigma f^2 + \frac{1}{2k^2} \left(\sigma f'^2 - \frac{2\ell}{r} f f' + \frac{\sigma \ell^2}{r^2} f^2 \right) \right] \text{Im} G_{\lambda\lambda}, \quad (9)$$

The optical force \mathbf{F} can be calculated from the energy shift via the well-known relation: $\mathbf{F} = -\text{Re} \nabla U$. After a significant amount of algebra we arrive at

$$\begin{aligned} \langle \mathbf{F}_{\text{EIMI}}^{\text{Circ}}(\mathbf{r}) \rangle = & \hat{\mathbf{r}} \frac{2I\sigma}{3\epsilon_0 c^2} \left(\frac{C_p^{|\ell|}}{w_0} \right)^2 \left(\frac{\sqrt{2}r}{w_0} \right)^{2|\ell|} e^{-\frac{2r^2}{w_0^2}} \left[\left(\frac{|\ell|}{r} - \frac{2r}{w_0^2} \right) L_p^{2|\ell|} - \frac{4r}{w_0^2} L_p^{|\ell|} L_{p-1}^{|\ell|+1} + \frac{1}{k^2} \left\{ \left(-\frac{\ell^2}{r^3} + \frac{|\ell|^3}{r^3} - \frac{4\ell^2}{rw_0^2} + \frac{8\ell\sigma|\ell|}{rw_0^2} - \frac{8\ell\sigma r}{w_0^4} \right. \right. \right. \\ & + \frac{6|\ell|r}{w_0^4} + \frac{2r}{w_0^4} - \frac{4r^3}{w_0^6} \left. \right\} L_p^{2|\ell|} + \left(\frac{16\ell\sigma|\ell|}{rw_0^2} - \frac{6|\ell|^2}{rw_0^2} - \frac{2\ell^2}{r^2 w_0^2} + \frac{24|\ell|r}{w_0^4} + \frac{8r}{w_0^4} - \frac{32\ell\sigma r}{w_0^4} - \frac{24r^3}{w_0^6} \right) L_p^{|\ell|} L_{p-1}^{|\ell|+1} \\ & \left. \left. + \left(\frac{8|\ell|r}{w_0^4} - \frac{16\ell\sigma r}{w_0^4} - \frac{16r^3}{w_0^6} \right) L_p^{|\ell|} L_{p-2}^{|\ell|+2} + \left(\frac{16|\ell|r}{w_0^4} + \frac{8r}{w_0^4} - \frac{16\ell\sigma r}{w_0^4} - \frac{32r^3}{w_0^6} \right) L_{p-1}^{|\ell|+1} - \frac{32r^3}{w_0^6} L_{p-1}^{|\ell|+1} L_{p-2}^{|\ell|+2} \right\} \right] \text{Im} G_{\lambda\lambda}. \quad (10) \end{aligned}$$

The potential energy (9) is plotted in Fig. 2 with the direction of forces \mathbf{F} (10) overlaid for the parallel $\ell = |\sigma|$ and antiparallel $\ell = -|\sigma|$ cases. This enantioselective trapping mechanism is quite similar to that of circularly polarized plane waves or 2D structured light, except in our system we have the spin-orbit-interactions (SOI) which occur in 3D fields³⁸ and these influence the helicity density distributions. For example, in the antiparallel case we produce an on-axis helicity density for $|\ell| = 1$. The influence the radial index p has on the enantioselective force is highlighted in Figure 3.

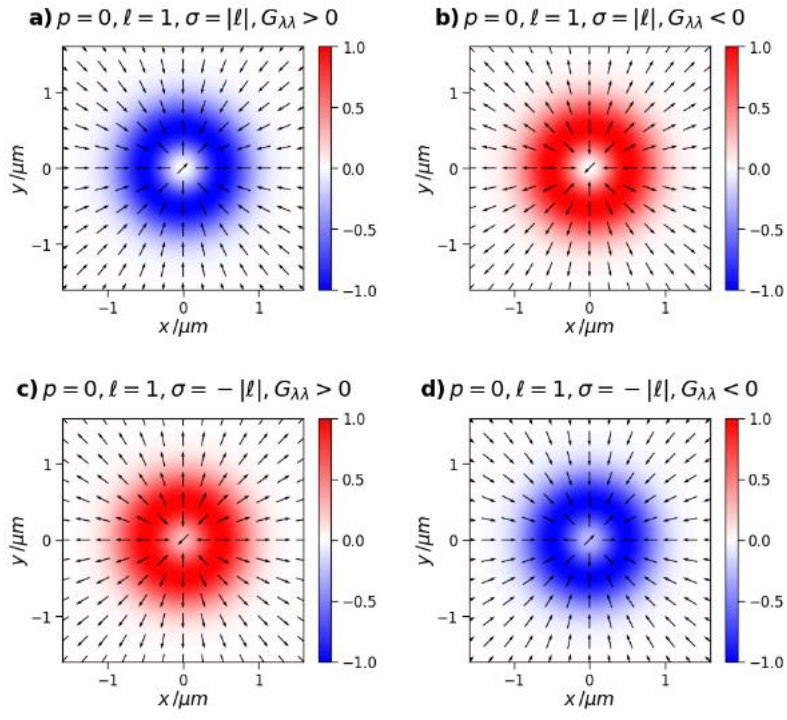


Figure 2: Individually normalized enantioselective potential energy (9) with forces overlaid (10) (arrows indicate only direction). $\lambda = w_0$ and $p = 0$ in all plots.

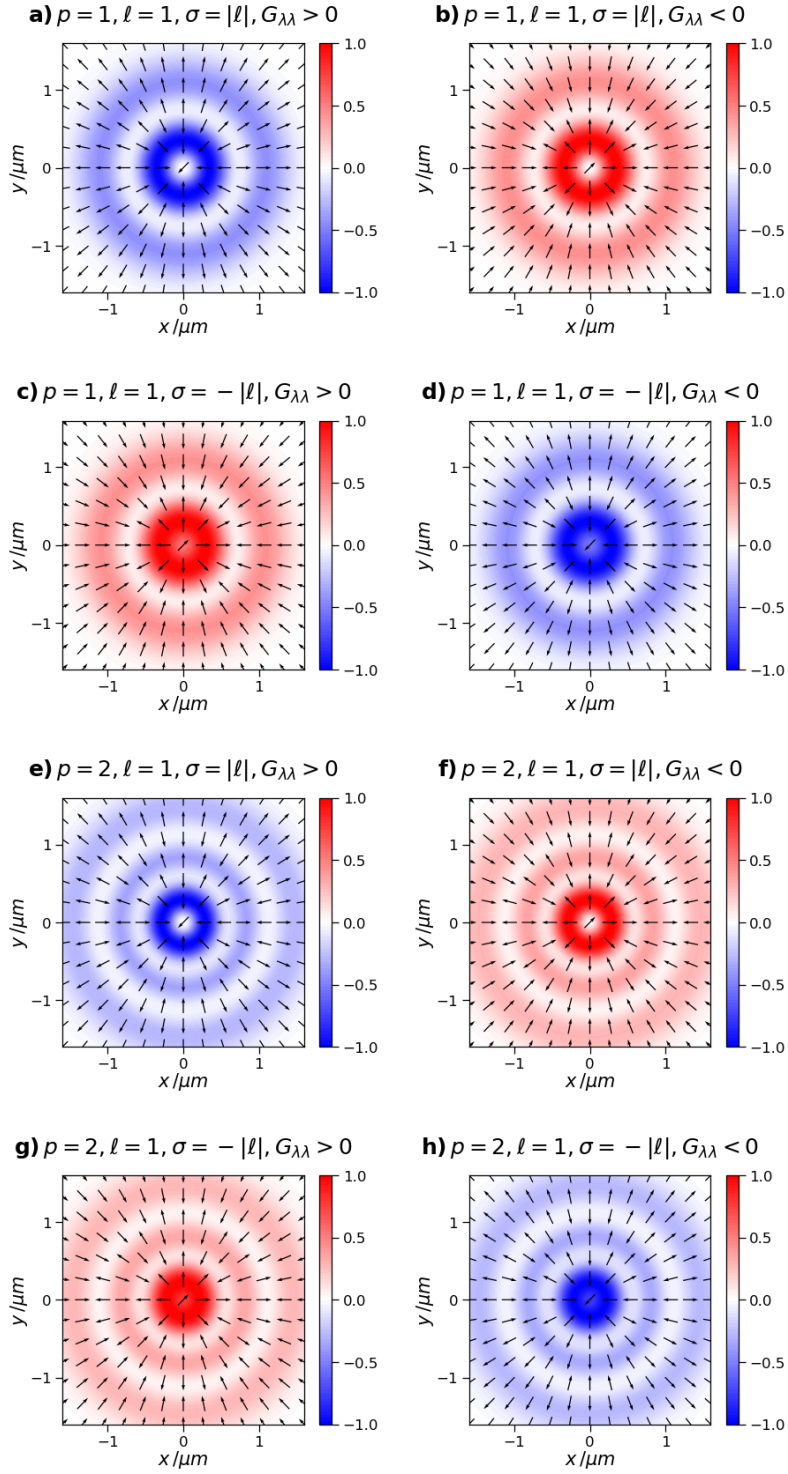


Figure 3: Influence of radial index p : individually normalized enantioselective potential energy (9) with forces overlaid (10) (arrows indicate only direction). $\lambda = w_0$ in all plots.

4. 2D POLARIZED INDEPENDENT ENANTIOSELECTIVE FORCE

The physics of the mechanism in the previous section is like predominantly all of the chiral enantioselective gradient force separation techniques to date which rely on the optical chirality of the 2D circular polarization state of the input beam. In this Section we outline the remarkable feature of 3D structured vortices in that they produce an enantioselective optical force that is independent of the 2D polarization state, i.e. even an input 2D unpolarized optical vortex which is tightly focused will produce an enantioselective gradient force in the focal plane. This is especially striking as the optical helicity/chirality of linearly polarized light has always been thought to be zero, let alone unpolarized light.

Optical helicity density h for propagating plane waves, 2D structured fields, and evanescent waves is proportional to the degree of 2D circular polarization of the input beam $h \propto \sigma$, being zero for linearly and randomly polarized inputs and taking on its maximum value for circular polarization. For linearly polarized and unpolarized plane waves there is no possibility for enantioselective gradient forces because $\sigma = 0$ and thus their optical helicity $h = 0$. In comparison, 3D structured LG modes are known to possess a non-zero optical helicity density contribution for 2D linear polarizations^{34,39} and it has recently been shown that remarkably this contribution is in fact independent of 2D polarization, being non-zero for even unpolarized input light⁴⁰. The rotationally averaged gradient trapping potential energy with an 2D unpolarized 3D LG input (i.e. the 2D polarization independent enantioselective trapping force) may be calculated by averaging (9) over the two orthogonal polarizations $\sigma = 1$ and $\sigma = -1$

$$\langle U_{\text{EIM1}}^{\text{ind}} \rangle = \frac{I}{3\epsilon_0 c^2} \frac{\ell}{k^2 r} \text{Im} G_{\lambda\lambda}. \quad (11)$$

The gradient forces acting on a chiral particle stemming from this 2D polarization independent potential energy are calculated as

$$\langle \mathbf{F}_{\text{EIM1}}^{\text{ind}} \rangle = \hat{\mathbf{r}} \frac{I}{3\epsilon_0 c^2} \left(\frac{C_p^{|\ell|}}{w_0} \right)^2 \left(\frac{\sqrt{2}r}{w_0} \right)^{2|\ell|} e^{-\frac{2r^2}{w_0^2}} \frac{8\ell}{k^2} \left[\left(\frac{|\ell|}{w_0^2 r} - \frac{r}{w_0^4} \right) L_p^{2|\ell|} + \left(\frac{2|\ell|}{w_0^2 r} - \frac{4r}{w_0^4} \right) L_p^{|\ell|} L_{p-1}^{|\ell|+1} - \frac{2r}{w_0^4} \left(L_{p-1}^{2|\ell|+1} + L_p^{|\ell|} L_{p-2}^{|\ell|+2} \right) \right] \text{Im} G_{\lambda\lambda}. \quad (12)$$

The potential energy (11) with the forces (12) overlaid at the focal plane $z = 0$ are shown in Fig. 4. It is important to make clear that these 2D polarization independent enantioselective forces are identical for either a 2D linearly polarized or 2D unpolarized 3D optical vortex. What the graphs show is that for a given sign of ℓ , the right-handed and left-handed chiral particles in an enantiomeric mixture are subject to discriminatory radial trapping forces which act to separate them into distinct rings in the transverse plane. For example, in Fig. 4a the enantiomer with $G > 0$ is pushed away from the beam axis and towards the blue (outer) ring, meanwhile in 4b it shows the $G < 0$ is pushed towards the central spot and away from the outer ring. The results are dependent on the sign of ℓ , and keeping everything else the same, for $-\ell$ the graphs in Fig 4. are the same but with the signs reversed. For example, for $-\ell$ the 4a $G > 0$ would look exactly like 4b.

Crucially both (11) and (12) stem purely from the longitudinal fields of (2) and (3), which means that the 3D structure of the optical vortex is essential and tight focusing is a must if the magnitudes of (11) and (12) are to be large enough to be observed experimentally.

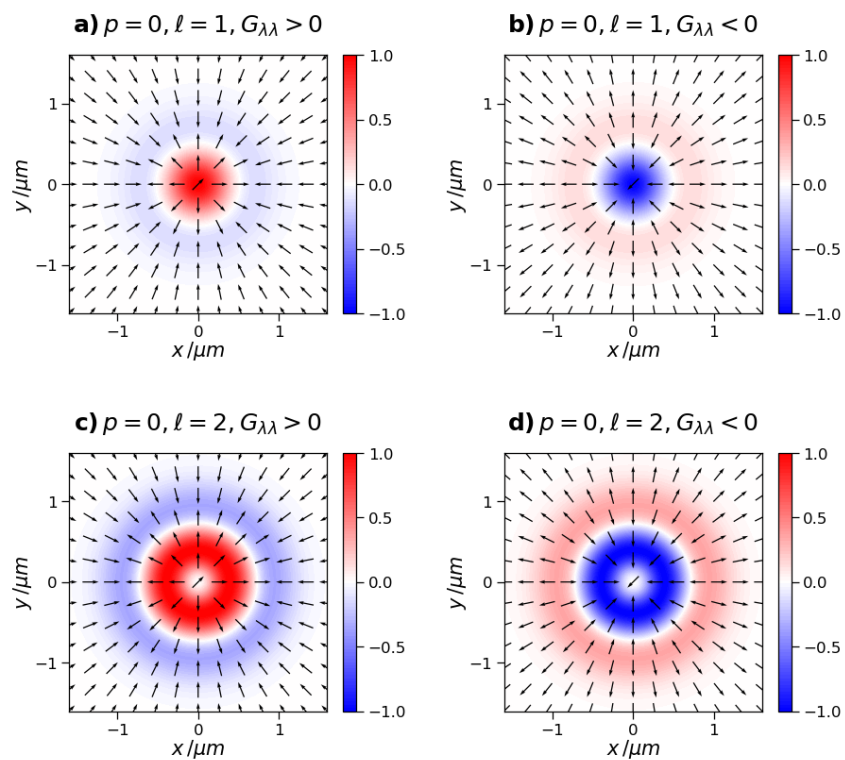


Figure 4: Individually normalized 2D polarization independent enantioselective potential energy (11) with vector optical force (12). Otherwise as Fig. 2.

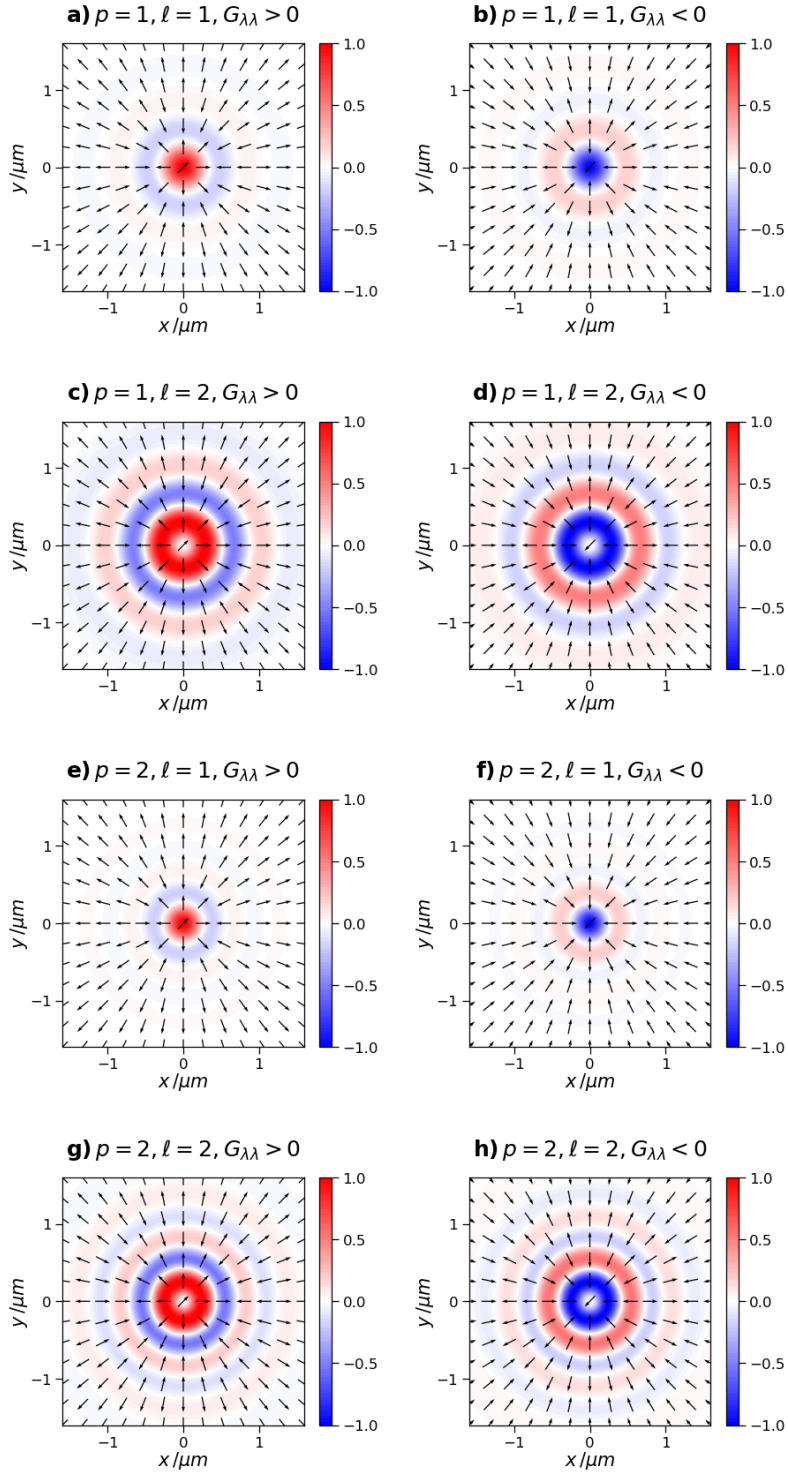


Figure 5: Individually normalized 2D polarization independent entioselective potential energy (11) with vector optical force (12). Otherwise as Fig. 3.

5. CONCLUSION

Evidently for natural chiral particles (e.g. molecules) the magnitudes of the forces involved will be small due their small $G_{\lambda\lambda}$ alongside the fact there will be present the dominant chirality-independent trapping potential U_{EIEI} from (6), however they are considered experimentally distinguishable^{41,42,1,10}, though are yet to be observed. Experimental realization of the fundamental mechanisms outlined here therefore have more potential in systems comprising of chiral nanoparticles or the use of plasmonic enhancement in nanophotonic setups^{16,43,44}. This work has provided further evidence of the significant potential of 3D structured light in light-matter interactions and nanophotonics. Explicitly, while enantiomer separation schemes utilizing the optical helicity of circularly polarized plane waves in gradient force mechanisms have been put forward^{8,10}, unlike 3D optical vortices, linearly polarized and unpolarized propagating plane waves possess no longitudinal fields or optical helicity and so the 2D polarization independent discriminatory force (12) could never have been envisaged under the plane wave approximation, nor a 2D structured light field.

ACKNOWLEDGEMENTS

KAF thanks the Leverhulme Trust for funding him through a Leverhulme Early Career Fellowship ECF-2019-398.

REFERENCES

1. Andrews, D. L. & Bradshaw, D. S. *Optical Nanomanipulation*. (Morgan & Claypool Publishers, 2017).
2. Jones, P. H., Maragò, O. M. & Volpe, G. *Optical tweezers: Principles and applications*. (Cambridge University Press, 2015).
3. Allen, L., Beijersbergen, M. W., Spreeuw, R. J. C. & Woerdman, J. P. Orbital angular momentum of light and the transformation of Laguerre-Gaussian laser modes. *Phys. Rev. A* **45**, 8185–8189 (1992).
4. Padgett, M. J. & Bowman, R. Tweezers with a twist. *Nat. Photonics* **5**, 343–348 (2011).
5. Woerdemann, M., Alpmann, C., Esseling, M. & Denz, C. Advanced optical trapping by complex beam shaping. *Laser Photonics Rev.* **7**, 839–854 (2013).
6. Yang, Y., Ren, Y., Chen, M., Arita, Y. & Rosales-Guzmán, C. Optical trapping with structured light: a review. *Adv. Photonics* **3**, 034001 (2021).
7. Forbes, A., de Oliveira, M. & Dennis, M. R. Structured light. *Nat. Photonics* **15**, 253–262 (2021).
8. Bradshaw, D. S. & Andrews, D. L. Chiral discrimination in optical trapping and manipulation. *New J. Phys.* **16**, 103021 (2014).
9. Bradshaw, D. S., Forbes, K. A., Leeder, J. M. & Andrews, D. L. Chirality in Optical Trapping and Optical Binding. *Photonics* **2**, 483–497 (2015).
10. Cameron, R. P., Barnett, S. M. & Yao, A. M. Discriminatory optical force for chiral molecules. *New J. Phys.* **16**, 013020 (2014).
11. Canaguier-Durand, A., Hutchison, J. A., Genet, C. & Ebbesen, T. W. Mechanical separation of chiral dipoles by chiral light. *New J. Phys.* **15**, 123037 (2013).

12. Lin, Z.-H., Zhang, J. & Huang, J.-S. Plasmonic elliptical nanoholes for chiroptical analysis and enantioselective optical trapping. *Nanoscale* **13**, 9185–9192 (2021).
13. Shi, Y. *et al.* Chirality-assisted lateral momentum transfer for bidirectional enantioselective separation. *Light Sci. Appl.* **9**, 1–12 (2020).
14. Ali, R., Pinheiro, F. A., Dutra, R. S., Rosa, F. S. & Neto, P. A. M. Enantioselective manipulation of single chiral nanoparticles using optical tweezers. *Nanoscale* **12**, 5031–5037 (2020).
15. Patti, F. *et al.* Chiral optical tweezers for optically active particles in the T-matrix formalism. *Sci. Rep.* **9**, 1–10 (2019).
16. Zhao, Y., Saleh, A. A. & Dionne, J. A. Enantioselective optical trapping of chiral nanoparticles with plasmonic tweezers. *ACS Photonics* **3**, 304–309 (2016).
17. Li, Y. *et al.* Enantioselective optical trapping of chiral nanoparticles using a transverse optical needle field with a transverse spin. *Opt. Express* **28**, 27808–27822 (2020).
18. Ding, K., Ng, J., Zhou, L. & Chan, C. T. Realization of optical pulling forces using chirality. *Phys. Rev. A* **89**, 063825 (2014).
19. Zheng, H., Chen, H., Ng, J. & Lin, Z. Optical gradient force in the absence of light intensity gradient. *Phys. Rev. B* **103**, 035103 (2021).
20. Tkachenko, G. & Brasselet, E. Helicity-dependent three-dimensional optical trapping of chiral microparticles. *Nat. Commun.* **5**, 4491 (2014).
21. Kravets, N., Aleksanyan, A., Chraïbi, H., Leng, J. & Brasselet, E. Optical Enantioseparation of Racemic Emulsions of Chiral Microparticles. *Phys. Rev. Appl.* **11**, 044025 (2019).
22. Fang, L. & Wang, J. Optical Trapping Separation of Chiral Nanoparticles by Subwavelength Slot Waveguides. *Phys. Rev. Lett.* **127**, 233902 (2021).
23. Chen, H., Liang, C., Liu, S. & Lin, Z. Chirality sorting using two-wave-interference–induced lateral optical force. *Phys. Rev. A* **93**, 053833 (2016).
24. Hayat, A., Mueller, J. P. B. & Capasso, F. Lateral chirality-sorting optical forces. *Proc. Natl. Acad. Sci.* **112**, 13190–13194 (2015).
25. Zhang, H. *et al.* Optical trapping two types of particles using a focused vortex beam. *Optik* **166**, 138–146 (2018).
26. Li, M., Yan, S., Zhang, Y., Zhang, P. & Yao, B. Enantioselective optical trapping of chiral nanoparticles by tightly focused vector beams. *JOSA B* **36**, 2099–2105 (2019).
27. Carretero, L., Acebal, P. & Blaya, S. Chiral Rayleigh particles discrimination in dynamic dual optical traps. *J. Quant. Spectrosc. Radiat. Transf.* **201**, 209–215 (2017).

28. Lu, W., Chen, H., Guo, S., Liu, S. & Lin, Z. Selectively transporting small chiral particles with circularly polarized Airy beams. *Opt. Lett.* **43**, 2086–2089 (2018).
29. Li, M., Yan, S., Zhang, Y., Chen, X. & Yao, B. Optical separation and discrimination of chiral particles by vector beams with orbital angular momentum. *Nanoscale Adv.* (2021) doi:10.1039/D1NA00530H.
30. Forbes, K. A. & Andrews, D. L. Orbital angular momentum of twisted light: chirality and optical activity. *J. Phys. Photonics* **3**, 022007 (2021).
31. Andrews, D. L., Bradshaw, D. S., Forbes, K. A. & Salam, A. Quantum electrodynamics in modern optics and photonics: tutorial. *JOSA B* **37**, 1153–1172 (2020).
32. Craig, D. P. & Thirunamachandran, T. *Molecular Quantum Electrodynamics: An Introduction to Radiation-Molecule Interactions*. (Courier Corporation, 1998).
33. Forbes, K. A., Green, D. & Jones, G. A. Relevance of longitudinal fields of paraxial optical vortices. *J. Opt.* **23**, 075401 (2021).
34. Forbes, K. A. & Jones, G. A. Measures of helicity and chirality of optical vortex beams. *J. Opt.* **23**, 115401 (2021).
35. Sheppard, C. J. Jones and Stokes parameters for polarization in three dimensions. *Phys. Rev. A* **90**, 023809 (2014).
36. Alonso, M. A. Geometric descriptions for the polarization for nonparaxial optical fields: a tutorial. *ArXiv Prepr. ArXiv200802720* (2020).
37. Andrews, D. L. Quantum formulation for nanoscale optical and material chirality: Symmetry issues, space and time parity, and observables. *J. Opt.* **20**, 033003 (2018).
38. Bliokh, K. Y., Rodríguez-Fortuño, F. J., Nori, F. & Zayats, A. V. Spin–orbit interactions of light. *Nat. Photonics* **9**, 796–808 (2015).
39. Woźniak, P., Leon, I. D., Höflich, K., Leuchs, G. & Banzer, P. Interaction of light carrying orbital angular momentum with a chiral dipolar scatterer. *Optica* **6**, 961–965 (2019).
40. Forbes, K. A. Optical helicity of unpolarized light. *Phys. Rev. A* **105**, 023524 (2022).
41. Bradshaw, D. S. & Andrews, D. L. Laser optical separation of chiral molecules. *Opt. Lett.* **40**, 677–680 (2015).
42. Bradshaw, D. S. & Andrews, D. L. Electromagnetic trapping of chiral molecules: orientational effects of the irradiating beam. *JOSA B* **32**, B25–B31 (2015).
43. Goerlitzer, E. S., Puri, A. S., Moses, J. J., Poulikakos, L. V. & Vogel, N. The Beginner’s Guide to Chiral Plasmonics: Mostly Harmless Theory and the Design of Large-Area Substrates. *Adv. Opt. Mater.* 2100378 (2021).
44. Warning, L. A. *et al.* Nanophotonic Approaches for Chirality Sensing. *ACS Nano* **15**, 15538–15566 (2021).